Available online at www.sciencedirect.com
SCIENCE DIRECT®
PERGAMON
International Journal of Heat and Mass Transfer 46 (2003) 2381–2388
International Journal of HEAT and MASS TRANSFER
www.elsevier.com/locate/ijhmt

# Transport phenomena in the thin-film region of a micro-channel

Kyoungwoo Park, Kwan-Joong Noh, Kwan-Soo Lee *

*School of Mechanical Engineering, Hanyang University, 17 Haengdang-dong, Sungdong-ku, Seoul 133-791, South Korea*

Received 7 June 2002; received in revised form 22 November 2002

**Abstract**

A mathematical model to predict the flow and heat transfer characteristics for a thin film region of a micro-channel is proposed. Gradient of the vapor pressure and the capillary force are considered. The effects of channel height, heat flux and slip boundary condition at the solid–liquid interface are investigated. The length of the thin film region is calculated by comparing the magnitude of the capillary and disjoining pressures. The length and the thickness of the thin film region decrease exponentially with increasing heat flux. The channel height has no effect on the shape of film thickness. In the case of slip condition, the decreased film thickness causes the capillary and disjoining pressures to increase.


## 1. Introduction

The capillary pumped loop (CPL) system using a phase-change technique to improve the heat transfer rate has drawn much attention to the electronic cooling applications. Recently, it has become more important to remove the heat generated in micro-scale devices as the advancement of packaging technology has led to the miniaturization of electronic components. The micro-CPL system is generally composed of the evaporator, condenser and vapor and liquid lines.

As shown in Fig. 1, when a liquid is in contact with a solid surface, the extended meniscus is divided into three parts [1]: (1) the intrinsic meniscus region, which is dominated by the capillary forces, (2) the thin film region, which is governed by both capillary and disjoining pressures, and (3) the adsorbed region, where the evaporation phenomenon does not occur.

In the last few decades, many efforts have been devoted to establishing the analytical models and conducting experiments for the performance of the extended meniscus region in various applications. Derjaguin et al. [2] were the first to analyze the thermo-fluid characteristics in the evaporating thin film region. They found that the solid–liquid molecular interactions in the thin film resulted in the liquid pressure reduction and the effect on the vapor pressure was relatively small. Potash and Wayner [3] studied the transport processes occurring in an evaporating extended meniscus in view of the physicochemical phenomena. They concluded that the liquid flows due to the disjoining pressure and the change of the meniscus curvature provided the necessary pressure gradient is present. Xu and Carey [4] conducted a combined analytical and experimental investigation on the liquid flow behavior in V-shaped micro-grooves. They suggested an analytical model that predicts the heat transfer characteristics of film evaporation, and found that the disjoining pressure differences may play a central role in the evaporation processes. Ha and Peterson [5] developed a theoretical model for the heat transfer characteristics of the evaporating thin liquid films in V-shaped micro-grooves with non-uniform input heat fluxes. Their results showed that when the dispersion number and the superheat are constant, the main factor affecting the length of the evaporating interline region is the heat flux supplied to the bottom of the plate. Kobayashi et al. [6] investigated theoretically and

* Corresponding author. Tel.: +82-2-2290-0426; fax: +82-2-2295-9021.
*E-mail address:* ksleehy@hanyang.ac.kr (K.-S. Lee).

0017-9310/03/$ - see front matter © 2003 Elsevier Science Ltd. All rights reserved.
doi:10.1016/S0017-9310(02)00541-0

**Nomenclature**

| | |
|---|---|
| $\bar{A}$ | dispersion constant (J) |
| $\bar{h}$ | average heat transfer coefficient, in Eq. (17) |
| $H$ | channel height (m) |
| $h_{fg}$ | latent heat of vaporization (J/kg) |
| $k$ | thermal conductivity (W/m K) |
| $K$ | curvature ($m^{-1}$) |
| $L$ | length of thin film region (m) |
| $\dot{m}$ | mass flow rate per unit width (kg/s m) |
| $\dot{m}''_{ev}$ | evaporating mass flow rate (kg/s $m^2$) |
| $P$ | pressure (Pa) |
| $q''$ | heat flux ($W/m^2$) |
| $u$ | velocity of $x$-direction (m/s) |
| $x$, $y$ | axial and vertical coordinate (m) |
| $z$ | new axial coordinate, $L - x$ |

*Greek symbols*

| | |
|---|---|
| $\beta$ | slip coefficient (m) |
| $\gamma$ | strain rate ($s^{-1}$) |
| $\delta$ | film thickness (m) |
| $\mu$ | viscosity (N s/$m^2$) |
| $v$ | kinetic viscosity ($m^2$/s) |
| $\rho$ | density ($kg/m^3$) |
| $\sigma$ | surface tension (N/m) |
| $\tau$ | shear stress ($N/m^2$) or time scale (s) |

*Subscripts*

| | |
|---|---|
| 0 | junction of thin film region and adsorbed region |
| c | capillary or critical |
| d | disjoining |
| i | liquid–vapor interface |
| l | liquid |
| L | junction of meniscus region and thin film region |
| v | vapor |

experimentally the evaporating heat and mass transfer phenomena at the vicinity of the liquid meniscus edge in the evaporator of a groove-type heat pipe. The results showed that a large heat flux is transported in the narrow micro-region.

Fluid modeling of Newtonian flow passing over a solid surface requires some assumptions about the nature of fluid mechanics. One of the fundamental assumptions is the no-slip condition on the wall. While this condition has been proven experimentally to be accurate for a number of types of flow at the macroscopic level, it often leads to unrealistic behavior at the microscopic level [7]. For liquids in micro-scales, Loose and Hess [8] suggested that if the strain rate at the wall exceeds twice the molecular frequency scale, the no-slip boundary condition at the wall leads to incorrect results.

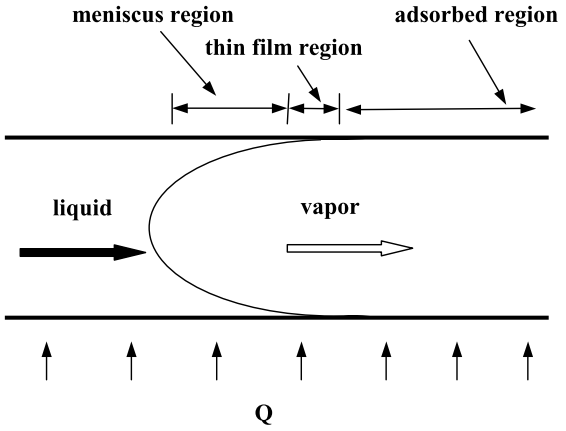


Fig. 1. Physical system of a micro-channel with the heat flux.

As the high heat transport rate occurs in the process of evaporation in the thin film region, a number of investigations have been conducted for this region. However, in most of these studies, the effect of vapor flow was neglected (i.e. the vapor pressure was assumed to be constant), some of them ignored the capillary pressure effect, and the transport phenomena were obtained by using the no-slip boundary condition at the solid–liquid interface.

The main purpose of the present study is to obtain the new mathematical model for the thin film region of the evaporator in a micro-channel and to investigate the effects of the parameters such as the input heat flux, the channel height and the slip boundary condition on the flow and heat transfer characteristics.

## 2. Theoretical analysis

The geometrical configuration and the coordinate system for the evaporating thin film flow in a micro-channel are shown in Fig. 2. The present mathematical model includes the gradient of the vapor pressure in the flow and the capillary force at the liquid–vapor interface. We consider only the lower half of the micro-channel because of the geometric symmetry. The following assumptions are employed in the derivation of the governing equations:

- a steady-state two-dimensional laminar flow,
- incompressibility of the liquid and the vapor,
- negligibly small convective terms in the momentum equation,

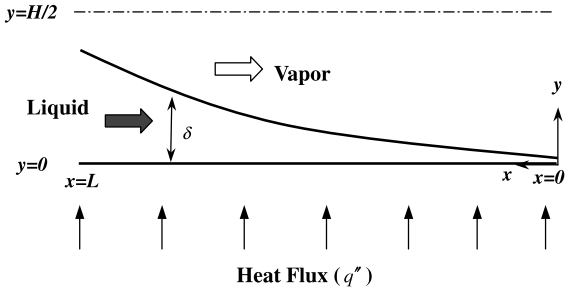


Fig. 2. Schematics and coordinate system for the thin film region.

- constant fluid properties and surface tension, and
- evaporation occurring only in the thin-film region.

### 2.1. Mathematical modeling

In the thin film region, the pressure difference between the vapor and liquid phases at the liquid–vapor interface is due to both the capillary ($P_c$) and disjoining pressures ($P_d$) and it can be expressed as

$$P_v - P_l = P_c + P_d \tag{1}$$

The capillary pressure is defined as the product of the interfacial curvature, $K$ and the surface tension, $\sigma$. The curvature of the interface can be expressed as

$$K = \frac{d^2\delta}{dx^2}\left[1 + \left(\frac{d\delta}{dx}\right)^2\right]^{-1.5} \tag{2}$$

The disjoining pressure results from the van der Waals forces, and relates the film thickness of non-polar liquids [2]. The disjoining pressure is expressed as

$$P_d = \frac{\bar{A}}{\delta^3} \tag{3}$$

where $\bar{A}$ is a dispersion constant (or Hamaker constant) and $\delta$ is the film thickness.

Combining Eqs. (1)–(3), and differentiating it with respect to $x$, then we obtain the following differential equation for $\delta(x)$:

$$\frac{d^3\delta}{dx^3} - 3\left(\frac{d\delta}{dx}\right)\left(\frac{d^2\delta}{dx^2}\right)^2\left[1 + \left(\frac{d\delta}{dx}\right)^2\right]^{-1} - \frac{1}{\sigma}\left(\frac{dP_v}{dx} - \frac{dP_l}{dx} + \frac{3\bar{A}}{\delta^4}\frac{d\delta}{dx}\right)\left[1 + \left(\frac{d\delta}{dx}\right)^2\right]^{-1.5} = 0 \tag{4}$$

As seen in Eq. (4), the liquid and vapor pressures must be obtained first to obtain the film thickness profiles.

The momentum equation for the liquid in the thin film region can be approximated by the lubrication theory,

$$\frac{d^2u_l}{dy^2} = \frac{1}{\mu_l}\frac{dP_l}{dx} \tag{5}$$

The criterion for applying the slip-flow condition in liquids was proposed by Loose and Hess [8]. In this work, the Navier's partial slip boundary condition [9], which assumes that the velocity at solid wall is proportional to the strain rate at the surface, is taken as

$$u_w = \beta\left.\frac{du}{dy}\right|_w \tag{6}$$

where $\beta$ is the slip coefficient. If $\beta$ is equal to zero, then no slip boundary condition is obtained.

The velocity profile for the liquid phase ($u_l$) is obtained by solving Eq. (5) with the boundary conditions of shear stress at the liquid–vapor interface and Navier's hypothesis of Eq. (6) at the wall. It can be given as follows:

$$u_l = -\frac{1}{2\mu_l}\left(\frac{dP_l}{dx}\right)(2\delta y - y^2) - \frac{\tau_i}{\mu_l}y - \frac{\beta}{\mu_l}\left(\delta\frac{dP_l}{dx} + \tau_i\right) \tag{7}$$

where $\tau_i$ is the shear stress at the liquid–vapor interface. The slip coefficient, $\beta$ can be obtained from the following equation which is proposed by Thompson and Troian [10].

$$\beta = \beta_0(1 - \gamma/\gamma_c)^{-1/2} \tag{8}$$

where $\beta_0$ is the limiting slip length and $\gamma_c$ represents the critical value of the shear rate. The slip coefficient under the condition of this study turns out to be approximately $5 \times 10^{-9}$ m.

The liquid pressure gradient is obtained by using Eq. (7) and the definition of $\dot{m}_l = \int_0^\delta \rho_l u_l\,dy$,

$$\frac{dP_l}{dx} = -\left\{\dot{m}_l + \frac{\delta}{\nu_l}\left(\frac{\delta}{2} + \beta\right)\tau_i\right\} \Big/ \left\{\frac{\delta^2}{\nu_l}\left(\frac{\delta}{3} + \beta\right)\right\} \tag{9}$$

The shape of momentum equation for $u_v$ is the same form as Eq. (5). The liquid is assumed to flow toward the vapor phase by evaporation at the liquid–vapor interface ($y = \delta$) and zero velocity gradient at the centerline ($y = H/2$) is also applied. Thus, $u_v$ can be obtained as

$$u_v = -\frac{1}{2\mu_v}\left(\frac{dP_v}{dx}\right)y^2 - \frac{H}{2\mu_v}\left(\frac{dP_v}{dx}\right)y + u_\delta - \frac{\delta}{2\mu_v}(\delta - H)\left(\frac{dP_v}{dx}\right) \tag{10a}$$

where $u_\delta$ is the velocity at $y = \delta$ and is given by

$$u_\delta = u_l|_{y=\delta} = -\frac{1}{2\mu_l}\left(\frac{dP_l}{dx}\right)\delta^2 - \left(\frac{\tau_i}{\mu_l} + \frac{\beta}{\mu_l}\frac{dP_l}{dx}\right)\delta - \frac{\beta}{\mu_l}\tau_i \tag{10b}$$

At the liquid–vapor interface, the shear stress for the vapor phase is equal to that of the liquid phase. Therefore, the vapor shear stress at $y = \delta$ is calculated as

$$\tau_i = \mu_l \left.\frac{\partial u_l}{\partial y}\right|_{y=\delta} = \mu_v \left.\frac{\partial u_v}{\partial y}\right|_{y=\delta} = \left(\delta - \frac{H}{2}\right)\left(\frac{dP_v}{dx}\right) \quad (11)$$

Combining Eqs. (10) and (11), and using the definition of $\dot{m}_v = \int_\delta^{H/2} \rho_v u_v \, dy$, the pressure gradient for vapor can be obtained as

$$\frac{dP_v}{dx} = -\left(\dot{m}_v + \frac{\rho_v H}{2} u_\delta\right) \Big/ \left\{ \frac{H^3}{24 v_v} + \frac{H\delta}{4 v_v}(\delta - H) \right\} \quad (12)$$

Substitution of Eq. (11) into Eq. (9) yields

$$\frac{dP_l}{dx} = -\left\{ \dot{m}_l + \frac{\delta}{v_l}\left(\frac{\delta}{2} + \beta\right)\left(\frac{dP_v}{dx}\right)\left(\delta - \frac{H}{2}\right) \right\} \Big/ \left\{ \frac{\delta^2}{v_l}\left(\frac{\delta}{3} + \beta\right) \right\} \quad (13)$$

The heat fluxes are specified as the input data. For the steady state condition, the net mass flow rate of vapor at $x = L$ (i.e., the junction of the thin film and the meniscus regions) must be zero, i.e., $\dot{m}_v(L) = 0$. Therefore, for constant $q''$, we have

$$\dot{m}_v(x) = \frac{\int_0^{L-x} q'' dx}{h_{fg}}, \quad \dot{m}_l(x) = \frac{\int_0^x q'' dx}{h_{fg}} \quad (14)$$

where $h_{fg}$ represents the latent heat of vaporization.

### 2.2. Boundary conditions

The governing equation for the film thickness, Eq. (4), is a third-order non-linear ordinary differential equation. The five boundary conditions for the film thickness, vapor and liquid pressures at $x = 0$ are as follows:

$$\delta|_{x=0} = \delta_0, \quad \left.\frac{d\delta}{dx}\right|_{x=0} = 0, \quad \left.\frac{d^2\delta}{dx^2}\right|_{x=0} = 0 \quad (15a)$$

$$P_{v,0} = P_{v,sat}(T_{v,0}), \quad P_{l,0} = P_{v,0} - \frac{\bar{A}}{\delta_0^3} - \sigma K \quad (15b)$$

In an ideal case, the film thickness at $x = 0$ (i.e., $\delta_0$) is generally of the order of $10^{-9}$ m. Water is used as the working fluid at a saturation temperature of approximately 383 K.

### 2.3. Numerical procedures

To obtain the flow and thermal characteristics in the thin film region, we solve Eqs. (4), (12) and (13) with the boundary conditions, Eq. (15), using the Runge–Kutta–Fehlberg method. The length of the thin film region ($L$) should be defined and calculated correctly for the classification of the thin film region and the meniscus region. The length of thin film region is determined when the disjoining pressure is greater than or equal to the capillary force because the disjoining pressure becomes a dominant force in a thin film region. Once $L$ is calculated, the film thickness can be easily obtained.

## 3. Results and discussion

In this study, the flow and heat transfer characteristics such as the film thickness and the pressure variations in the thin film region have been investigated. The influences of the heat flux, the channel height, and the slip boundary condition at the solid–liquid interface have been also investigated numerically. The results presented in this paper are those for the no-slip boundary condition if additional explanation is not mentioned. Table 1 shows the basic properties of water as the working fluid.

### 3.1. Flow and thermal characteristics

Here, the channel height ($H$) is 150 μm and the heat flux ($q''$) is $10^6$ W/m$^2$. To investigate the influence of the vapor pressure gradient, the film thickness along the flow direction for the two cases (i.e., present study and $dP_v/dx = 0$) are shown in Fig. 3. A new independent variable, $z$, which is defined as $z = L - x$, is introduced

Table 1
Properties of $H_2O$ as the working fluid at 383 K

| Properties | Values |
|---|---|
| Dispersion constant ($\bar{A}$) | $2.87 \times 10^{-21}$ J |
| Latent heat of evaporation ($h_{fg}$) | $2.256 \times 10^6$ J/kg |
| Thermal conductivity of liquid ($k_l$) | 0.68 W/m K |
| Density of liquid ($\rho_l$) | 958.31 kg/m$^3$ |
| Viscosity of liquid ($\mu_l$) | $2.82 \times 10^{-4}$ N s/m$^2$ |
| Density of vapor ($\rho_v$) | 0.598 kg/m$^3$ |
| Viscosity of vapor ($\mu_v$) | $12.02 \times 10^{-6}$ N s/m$^2$ |
| Surface tension ($\sigma$) | $5.89 \times 10^{-2}$ N/m |

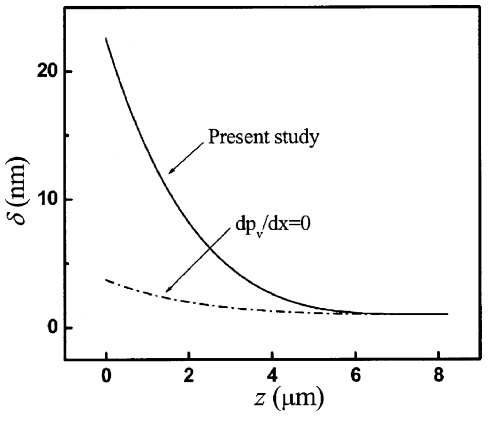


Fig. 3. Effect of the vapor pressure on the film thickness.

here. In most researches, the vapor pressure ($P_v$) was assumed to be constant for the sake of simplicity although it is obvious that the phase-change process of the working fluid causes variation of the vapor pressure. When compared with the present result, the film thickness with a constant vapor pressure is underestimated as shown in Fig. 3. Therefore, the vapor pressure should not be assumed to be constant. It is also found that the film thickness decreases exponentially as the liquid flows toward the adsorbed region. The profile of thin film is mainly influenced by the liquid evaporation, and the evaporation phenomenon causes the pressure gradient to decrease so that mass conservation has to be maintained. Therefore, the variation of film thickness can be easily explained by the following pressure distribution in the thin film region.

Fig. 4 shows the liquid and vapor pressure variations along the axial flow direction ($z$). The absolute value of the vapor pressure is much greater than that of the liquid pressure in the thin film region as shown in Eq. (15b). The variation of the liquid pressure is negligible small for $0 < z < 4$ μm and then it decreases sharply. On the contrary, the vapor pressure gradually decreases with $z$ and its variation is very small compared to that of the liquid pressure. This result means that the liquid and vapor phases flow in the same direction. The pressure difference between liquid and vapor phases is owing mainly to the liquid pressure because the gradient of vapor pressure is relatively small in the thin film region. From this fact, the variation of liquid pressure is more dominant factor than that of vapor pressure in formation of the thin film.

The distributions of capillary and disjoining pressures ($P_c$ and $P_d$) with $z$ are shown in Fig. 5. The capillary pressure, which has a maximum value at $z = 0$, decreases exponentially along the thin film region and its distribution has the same trend as that of the film thickness. But the disjoining pressure, which experiences no noticeable change at a minimum value for $z < 4$ μm, increases sharply to $z = 7$ μm and then maintains a maximum value until it reaches the adsorbed region. It is also found that the disjoining pressure shows a significant effect on the flow in the thin film region because its value is much greater than that of the capillary pressure as shown in the Fig. 5. Hence, many earlier researches have neglected the effect of capillary pressure in the thin film region [4,5].

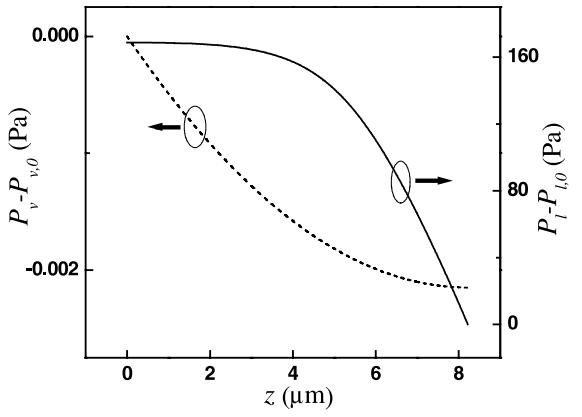


Fig. 4. The liquid and vapor pressure variations.

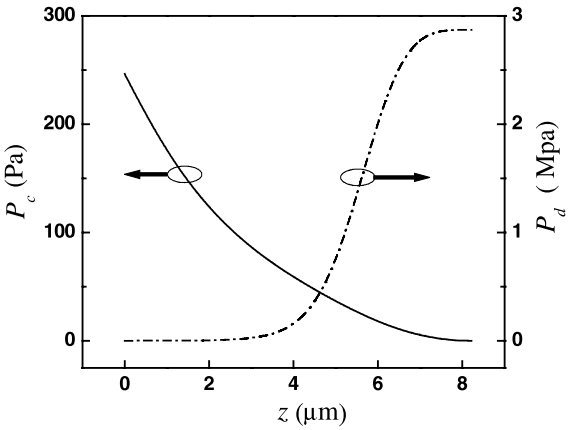


Fig. 5. The capillary and disjoining pressures.

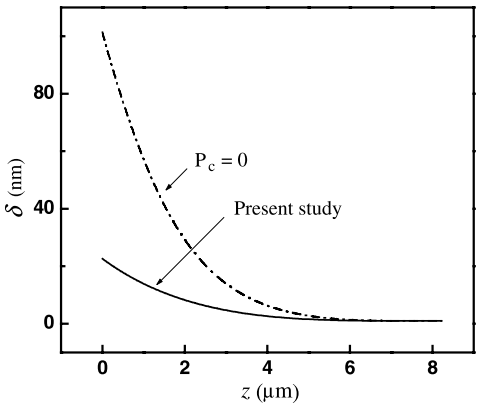


Fig. 6. Effect of the capillary pressure on the film thickness.

To investigate the effect of the capillary pressure on the film thickness, the film thickness for two cases (present study and $P_c = 0$ Pa) according to the flow direction is shown in Fig. 6. The distribution of film thickness with capillary pressure is indeed much flatter than the case of neglecting the capillary pressure. Therefore, the capillary pressure effect should be considered for more accurate results.

### 3.2. Effect of the heat flux

Fig. 7 presents the length of the thin film region ($L$), the maximum film thickness at $z = 0(\delta_L)$ and the

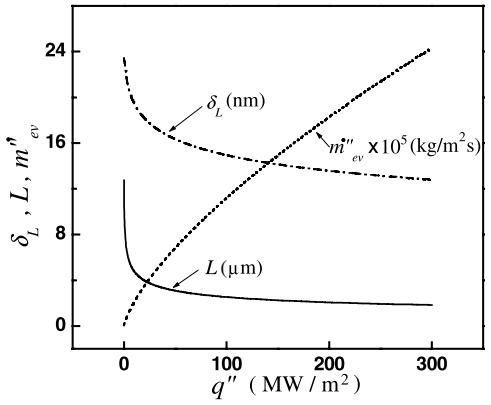


Fig. 7. Variation of the length of the thin film region, the maximum film thickness and the evaporating mass flux with the heat flux.

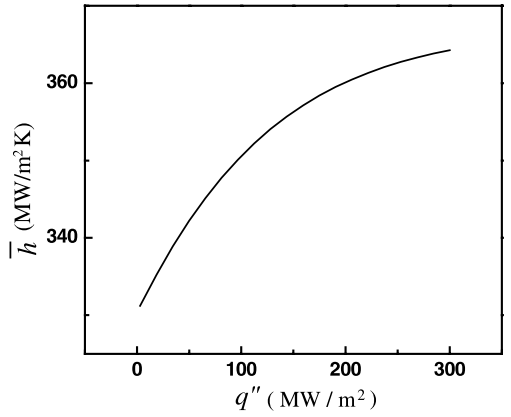


Fig. 8. The average heat transfer coefficient with the heat flux.

evaporating mass flux ($\dot{m}''_{ev}$) with various heat fluxes. In this study, the evaporating mass flux can be related to the liquid mass flow rate by the following mass balance:

$$\dot{m}''_{ev} = -\frac{d\dot{m}_l(x)}{dx} \tag{16}$$

Note that the direction of evaporating mass flux is normal to the liquid–vapor interface. As shown in Fig. 7, the length of the thin film region and the maximum thickness decrease as the heat flux increases. In particular, their gradients are much larger for $q'' < 10$ MW/m$^2$. This result is qualitatively in agreement with Ha and Peterson's result [5]. The supplied heat flux on the micro-channel has a little influence on the length of the thin film region for $q'' > 200$ MW/m$^2$. The decrease in the length of the thin film region and maximum film thickness with the heat flux is mainly due to the increase of the evaporating mass flux ($\dot{m}''_{ev}$). The evaporating mass flux increases linearly with increasing heat flux. If the evaporating mass flux increases, more liquid has to flow into the thin film region in order to maintain the law of mass conservation. This phenomenon can be mainly achieved by increasing the gradient of the liquid phase pressure.

To investigate the amount of heat transfer rate in the micro-channel quantitatively, the average heat transfer coefficient, $\bar{h}$, is defined as

$$\bar{h} = \frac{1}{x}\int_0^x h(x)\,dx \approx \frac{1}{L}\int_0^L \frac{k_l}{\delta(x)}\,dx \tag{17}$$

Fig. 8 illustrates the average heat transfer coefficient with the heat flux. As the heat flux increases, the average heat transfer coefficient increases. The increased heat flux causes an increase of evaporation at the liquid–vapor interface. The increased evaporation results in the decreases in both film thickness and maximum length of the thin film region. Therefore, the decrease of the film thickness decreases the thermal resistance in the thin film and causes the heat transfer to increase.

### 3.3. Effect of the channel height

The film thickness, the capillary pressure and the disjoining pressure according to the liquid flow direction for $H = 90$, 110, 130 and 150 μm are shown in Fig. 9(a) and (b), respectively. The shape of the film thickness remains unchanged regardless of the variation of channel height. The length of the thin film region and the film thickness decreases as the channel height decreases. This is due to the fact that the decreased channel height increases the mass flow rate in the liquid phase, and the increased mass flow rate increases the pressure gradient in both the liquid phase and the vapor phase. Fig. 9(b) shows that the location of sharp increase of the disjoining pressure moves closer to the inlet of the thin film region ($z = 0$) as the channel height decreases. It is also found that the capillary pressure increases with decreasing the channel height. This means that the effect of capillary pressure on the flow field increases as the channel height decreases because of the reduction of the curvature.

Fig. 10 shows the average heat transfer coefficient ($\bar{h}$) with the channel heights. As the channel height increases, the heat transfer decreases sharply in the region of $H \leqslant 50$ μm and then it decreases slightly. As mentioned earlier, the heat from the liquid phase to the vapor phase increases as the film thickness decreases gradually. It seems that the Navier–Stokes equation, with no-slip condition at the solid wall, cannot be used $H \leqslant 50$ μm because the strain rate increases with the decreasing in channel height, which causes $\gamma \geqslant 2\tau^{-1}$ to be satisfied. This means that when the no-slip condition is applied at the liquid–solid interface for $H \leqslant 50$ μm, the solution may be unstable.

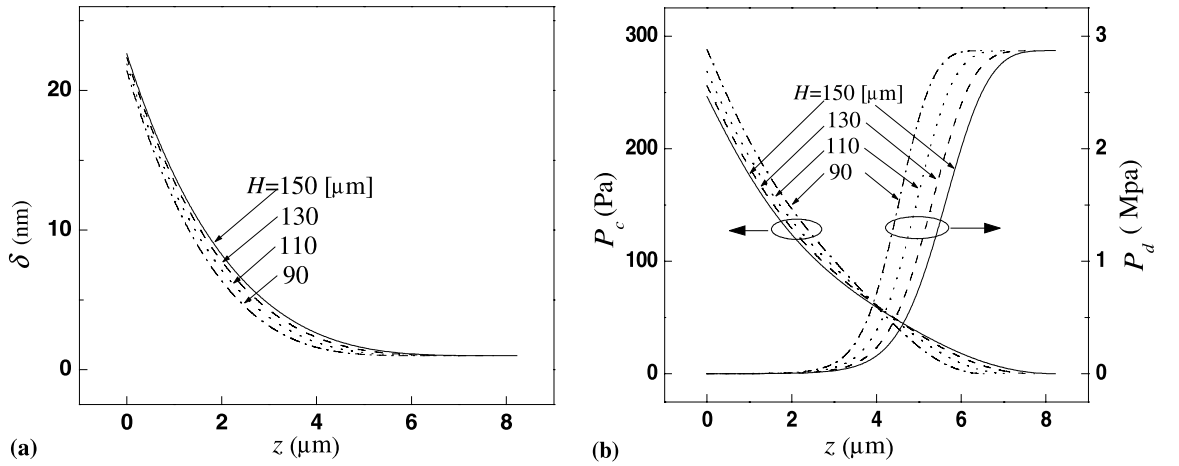


Fig. 9. The effect of channel height on the flow in the thin film region: (a) the film thickness and (b) the capillary and disjoining pressures.

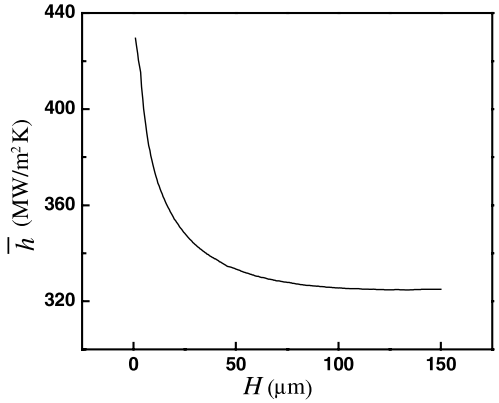


Fig. 10. The average heat transfer coefficient with the channel height.

### 3.4. Effect of the slip boundary condition

Fig. 11 shows the liquid film thickness and the capillary and disjoining pressures along the liquid flow direction for the channel height of 50 μm and the heat flux of $10^6$ W/m$^2$. When the slip condition at the liquid–solid interface is considered, the film thickness is decreased and the length of thin film region becomes shorter compared with those for the no-slip condition as shown in Fig. 11(a). This is due to the fact that the liquid flows faster and the gradient of liquid pressure, in turn, increases compared with that of the no-slip condition. Fig. 11(b) shows that the capillary pressure becomes higher than that of the no-slip condition. This is mainly due to the increase in curvature $K$ for the same $z$-locations under the constant surface tension, as shown in

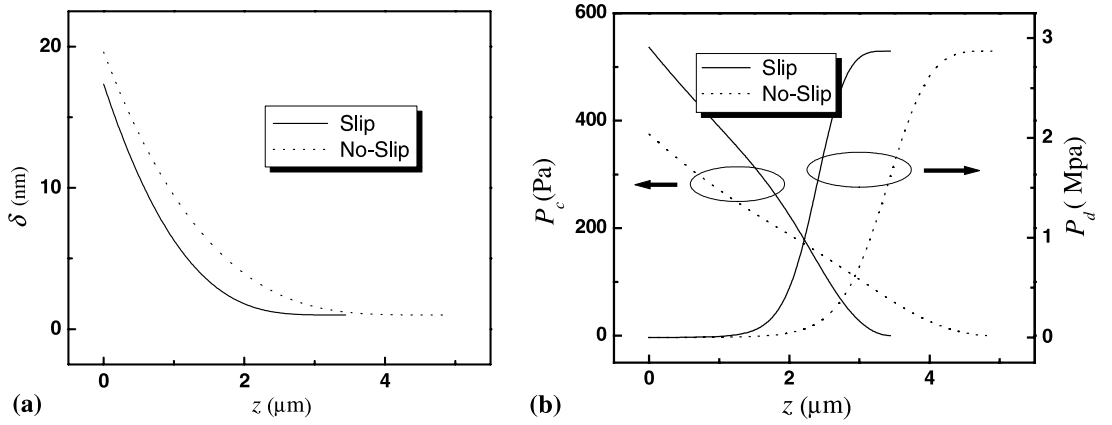


Fig. 11. The effect of slip-boundary condition on the flow in the thin film region at $H = 50$ μm and $q'' = 10^6$ W/m$^2$ K: (a) the film thickness and (b) the capillary and disjoining pressures.

Fig. 11(a). The disjoining pressure for the slip-flow condition is higher than that of the no-slip condition due to the decreased film thickness.

## 4. Conclusions

A mathematical model considering the gradient of vapor pressure in the flow and capillary force at the liquid-vapor interface is presented to investigate the two-phase flow and heat transfer phenomena in the evaporating thin film region of a two-dimensional micro-channel. The effects of the heat flux, the channel height, and the slip boundary condition at the solid-liquid interface are investigated.

The shape and thickness of the thin film in a micro-channel is influenced by the gradient of vapor pressure. The capillary force must be considered for more accurate results although its value is relatively small compared to the disjoining pressure. As the heat flux increases, the length and the maximum thickness of the thin film decrease exponentially and the local evaporating mass flux increases linearly. With decreasing the channel height, the length and film thickness of the thin film decrease and the effect of the capillary force increases gradually. However, there is little effect of the channel height on the shape of the film thickness.

In the case of the slip condition, the length and film thickness of the thin film are decreased compared with those of the no-slip condition, and the decreased film thickness cause the capillary and disjoining pressures to increase.

## Acknowledgements

This research was supported by The Center of Innovative Design Optimization Technology (iDOT), Korea Science and Engineering Foundation.

## References

[1] F.W. Holm, S.P. Goplen, Heat transfer in the meniscus thin-film region, ASME J. Heat Transfer 101 (1979) 498–503.
[2] B.V. Derjaguin, S.V. Nerpin, N.V. Churaev, Effect of film transfer upon evaporating liquids from capillaries, RILEM Bull. 29 (1965) 93–98.
[3] M. Potash Jr., P.C. Wayner Jr., Evaporation from a two-dimensional extended meniscus, Int. J. Heat Mass Transfer 15 (1972) 1851–1863.
[4] X. Xu, V.P. Carey, Film evaporation from a micro-grooved surface-an approximate heat transfer model and its comparison with experimental data, AIAA J. Thermophys. Heat Transfer 4 (1990) 512–520.
[5] J.M. Ha, G.P. Peterson, The interline heat transfer of evaporating thin film along a micro grooved surface, ASME J. Heat Transfer 118 (1996) 747–755.
[6] Y. Kobayashi, S. Ikeda, M. Iwasa, Evaporative heat transfer at the evaporative section of a grooved heat pipe, J. Thermophys. Heat Transfer 10 (1996) 83–89.
[7] J. Koplik, J.R. Banavar, Corner flow in the sliding plate problem, Phys. Fluids 7 (1995) 3118–3125.
[8] W. Loose, S. Hess, Rheology of dense fluids via nonequlibrium molecular hydrodynamics: Shear thinning and ordering transition, Rheologica Acta 48 (1989) 91–101.
[9] S. Goldstein, in: Modern Developments in Fluid Dynamics, vol. 2, 1965, p. 676.
[10] P.A. Thompson, S.M. Troian, A general boundary condition for liquid flow at solid surfaces, Nature 389 (1997) 360–362.